DISTRIBUTION STATEMENT A. Approved for public release; distribution is unlimited.

Biological Response to the Dynamic Spectral-Polarized Underwater Light Field

PI: Molly E. Cummings
Integrative Biology Department
University of Texas
Austin, TX 78712
phone: (512) 471-3499 fax: (512) 471-3878 email: mcummings@austin.utexas.edu

Co-PI: Samir Ahmed (City College of New York)
Co-PI: Heidi Dierssen (University of Connecticut)
Co-PI: Alexander Gilerson (City College of New York)
Co-PI: William F. Gilly (Stanford University)
Co-PI: George Kattawar (Texas A & M University)
Co-PI: Brad Seibel (University of Rhode Island)
Co-PI: James Sullivan (University of Rhode Island)

Award Number: N000140911054
http://www.bio.utexas.edu/research/cummingslab/

LONG-TERM GOALS

Camouflage in marine environments requires matching all of the background optical properties: spectral, intensity and polarization components─ all of which can change dynamically in space and time. Current research suggests that polarization detection is more sensitive than other conventional detection methods in scattering media such as the ocean, hence underscoring the need to develop polarized camouflage technology. Our research investigates the biological challenge of camouflage in the near-shore littoral zone and near-surface marine environments in two distinct water types found in coastal environments around the globe (oligotrophic and eutrophic) with particular emphasis on the polarization properties. We aim to characterize the dynamic light field along with the behavioral and cellular response of camouflaging animals in these environments. Our long-term goal is to identify the biological pathways for concealment against the underwater spectral-polarized light field enabling us to identify design principles for future naval camouflage.

OBJECTIVES

(1) Measure and model the spectral-polarized light field in near-shore and near-surface environments

(2) Characterize the biological camouflage response of organisms to these dynamic optical fields

(3) Identify the internal controls and structural mechanisms that coordinate the camouflage response

APPROACH

Our first aim is to **measure and model the underwater spectral-polarized light field in distinct water types.** We characterize the light field by the simultaneous deployment of a comprehensive optical suite including underwater video-polarimetry (full Stokes vector video-imaging camera custom-built (Cummings), and "SALSA" (Bossa Nova Technologies, CA) Gilerson), inherent optical properties (MASCOT, Sullivan), hyper-spectral multi-angular Stokes vector spectroradiometry (Gilerson,Ahmed), and hyperspectral benthic reflectance (Dierssen). These measurements will be used to refine development of, and make comparisons to, theoretical expectations from a fully 3-D radiative transfer model that solves for each of the polarization elements of the Mueller matrix transformation of the Stokes vector by (Kattawar). The first modeling objective of this proposal is to calculate the complete Mueller matrix/Stokes vector for any set of oceanic and atmospheric conditions for any region of the ocean. We will then use this modeling approach (i) to predict the 3-D light field; (ii) to calculate experimental conditions to measure biological responses; and (iii) to investigate the nature of the light field as it interacts with cells within the skin. Our approach is to develop a 3-D Monte Carlo model with full Mueller matrix treatment.

During field operations, we couple polarimetry measurements of live, free-swimming animals in their environments with a full suite of optical measurements (mentioned above) to completely characterize the **biological response to dynamic optical environments** (Cummings, Gilerson, Dierssen, Sullivan, Seibel, Ahmed). We also restrain live, awake animals to take polarimetry measurements (in the field and laboratory) under a complete set of viewing angles and incident polarization light fields. We use Mueller matrix modeling to determine the specific Mueller matrix elements of animals that differ from those of conventional structures currently deployed for open ocean camouflage (e.g. standard mirror). Furthermore, we examine in vivo "flickering" activity on the skin of squid and its relationship to background matching (wave-induced fluctuations of the light field) (Gilly). We also develop new numerical approaches to quantify organismal pattern in relationship to the background (Dierssen).

We **identify the internal control of these field-studied organisms and structural mechanisms that coordinate the camouflage response** by (a) characterizing different tissue layers and organelles associated with different species occupying a diverse array of marine habitats using a combination of light and SEM microscopy (Cummings, Gilly), (b) examining both iridophore and chromatophore control processes and the local vs peripheral control features using both pharmacological and electrical stimulation techniques (Gilly, Cummings), and (c) developing a novel 3D Monte Carlo model to describe how the spectral-polarized light field interacts with cells within the skin (Kattawar).

WORK COMPLETED

a) Published group paper examining the biological structural mechanisms of polaro-crypsis and broadband reflectance in the Lookdown, *Selene vomer*. (Cummings, Kattawar; Zhao et al 2015)

b) Submitted and revised group paper examining in nature camouflage strategies of open ocean fish as compared to nearshore fish in epipelagic waters (Cummings, Kattawar, Sullivan, Dierssen, Twardowski, Gilerson; Brady et al. *in press Science*).

c) Revised paper examining differences in polarization reflectance between species of different optical habitats, and peripheral vs central control of fish polarization reflectance. (Cummings)

d) Continued field measurements (East Sound, WA) of the optical properties of different environments to better understand and model the effects of different particle fields on the resulting VSF and polarized light field synergistic to the goals of the MURI project and in conjunction with the Naval Research Laboratory, Stennis, MS (Sullivan, Twardowski, Kattawar).

e) Two joint research cruises with NRL were conducted in 2015, where in-situ holography of the particle field, in-situ and boat mounted scanning LIDARs and in-situ polarized scattering (both linear and circular) were measured simulateously in the same optical plane. (Sullivan, Twardowski, Kattawar). These data are the first of its kind and may validated optical modeling work currently being conducted by Kattawar both for the MURI and a related ONR sponsored project.

f) Published paper on background matching in the Sargassum crab (Dierssen; Russell et al. 2015)

g) We developed a matlab toolbox to quantify spatial patterns of an organism from an image using both a texture and mutual information approach (Dierssen; Brown et al. in prep)

h) Published paper on in situ color-changing behaviors of Humboldt squid (Dosidicus gigas) filmed with an animal-borne video package (Rosen, Gilly, et al. 2015. Journal of Experimental Biology).

i) Presented talk at the Animal Behavior Society annual meetings (Anchorage, Alaska): "Polarization Signaling: how fish hide and dynamically communicate with polarized light" (Cummings)

j) Presented talk at the International Conference Behaviour 2015 (Cairns, Australia) entitled "Quantifying polarocrypsis of silvery fish in the open ocean through massively multi angular measurements" (Cummings, Brady)

RESULTS

1) In field videopolarimetry measurements (>1500) of live fish and man-made surfaces (specular and diffuse mirrors) in near surface open ocean environments reveal that open ocean carangid fish reflectance provides greater overall polarization and intensity camouflage than either nearshore fish species or man-made mirror surfaces (Fig 1). Continuous azimuthal measurements of fish and surfaces against background water were collected as well as different viewing angles (camera positioned above, below and in line with fish; and fish in different positions relative to camera). This study identifies that optimal crypsis in the open ocean requires different types of surface reflectance at different viewing angles, and that open ocean fish signicantly outperform mirrors at viewing angles relevant for predator detection and pursuit (data not shown). Furthermore this study identifies the structural arrangement of guanine platelets that enable open ocean carangid fish species to minimize contrast at many viewing angles (Data not shown; Brady et al., *in press* at *Science*; Cummings, Gilerson, Dierssen, Kattawar, Sullivan).

2) Pharmacological effects on chromatophore activity in *Dosidicus gigas* and *Doryteuthis (Loligo) opalelscens* were compared. Tetrodotoxin (TTX, 200 nM) blocked electrically stimulated activity in both species. Electrical stimulation is ineffective in chronically denervated (5-7 days) skin of *Doryteuthis*, spontaneous waves occur that are resistant to TTX. These results are consistent with the idea that spontaneous waves do not involve normal excitatory control mediated by the central nervous system. We propose that a peripheral mechanism allows excitation to spread between neighboring chromatophores in denervated *Doryteuthis* as well as

in intact *Dosidicus*, and that flickeirng in the living squid invovles this pathway. Serotonin (2.5 μM) has no major effect on electrically stimulated activity in intact *Doryteuthis*, but it inhibits to some degree in *Dosidicus*. 5HT eliminates spontaneous wave-like activity in both *Dosidicus* and denervated *Doryteuthis*. These results are consistent with a role for 5HT as an inhibitory modulator in the normal condition in both species and a lack of inhibition in the denervated condition following degeneration of serotonergic axons. (Gilly)

3) Labeling of actin with fluorescent phalloidin and examination using confocal microscopy in *Doryteuthis* (normal and denervated) and in *Dosidicus* reveals that radial muscle fibers in both species branch into fine processes at the distal ends. In some cases the distal processes of muscle fibers from neighboring chromatophores appear to be physically connected, particulary in *Dosidicus* (Figs. 2Aii and 2B). We propose that functional connections at these points provides a coupling mechanism for propagation of excitation through the chromatophore network in *Dosidicus* and denervated *Doryteuthis* that does not involve the normal excitatory neural pathway. In Dosidicus, 8% of muscle fibers show such a connection, but the figure is much smaller in *Doryteuthis* (0.2% of innervated muscle fibers and 0.78 ± 0.79% of 1,437 denervated fibers.) Labeling of neural processes with anti-glutamate and anti-5HT in *Doryteuthis* reveals axons that run together apposed to radial muscle fibers (Figs.2B,C). Chronic denervation leads to complete degeneration of the serotonergic axons in the denervated field (Fig. 2D). These results are consistent with a lack of serotonergic inhibition following denervation as proposed above. *Dosidicus* has a more sparse glutamateric excitatory innervation, and every muscle fiber does not appear to be directly innervated (Fig. 3B). Serotonergic axons are not associated with indiviudal radial muscle fibers, but a diffuse plexus of serotonergic processes is present (Fig. 3C). We propose that these serotonergic processes play an inhibitory role in *Dosidicus* but one that is weaker and perhaps qualitatively different than in *Doryteuthis*. (Gilly)

4) We used a 2D Finite-Difference Time Domain (FDTD) code to simulate the spectral reflectance of the iridophore system. Figure 4A shows a microscopic view of a 2D iridophore cell and 5 blue sub-regions are indicated by blue boxes. The iridosome (black) refractive index is 1.59, while medium(white) refractive index is 1.33. The predicted reflectance spectra are showed in Figure 3B. These reflectance peaks are caused by the coherent orientation of plates at certain wavelengths. Then we conducted the same simulations on the 2D circular region from a cuttlefish fin spot (the central circular region in Figure 5). The overall reflectance spectra at different incident angles are plotted as a colorful annulus in Figure 5. (Kattawar)

5) Simulation of the Optical Properties of an Oceanic Diatom: the optical properties of a chain-forming triangular prism oceanic diatom are studied in terms of the many-body iterative T-matrix (MBIT) method [Yan 2008, Sun 2013] and the ray-by-ray (RBR) geometric optics method [Yang 1997] (Fig 6). The Discrete Dipole Approximation (ADDA) is also employed to verify the simulation results (Fig 7). The MBIT, a numerically accurate method, is advantageous to deal with scatterers with large aspect ratios or consisting of a liner cells. The MBIT can be employed to get the optical properties of diatoms in small and intermediate sizes. The RBR, an approximated method, is taking the interferences of all outgoing rays into consideration, compared to other geometric optics methods. The RBR can be employed to get the optical properties of diatoms in intermediate and large sizes (Fig 8). A diatom cell is modeled as two concentric triangular prisms with two cylinders on the two ends and with a sphere in the center of the prisms, based on a SEM image of a diatom cell. The relative

refractive indices of the outer prism and two spines, the inner prism, and, the sphere are set to be 1.1+i0.0, 1.03+i0.0001, and 1.06+i0.025, respectively [Aas 1981, Aas 1996]. (Kattawar)

6) Microscope measurements of carangid fish (lookdown) reflectance layers reveals that the guanine platelet distribution along the vertical axis of the fish have a near uniform alignment but have a random distribution along the short axis of the fish, providing a selective reflectance and contributing to their polaro-crypsis. (Cummings, Kattawar, Figs 9,10). The reflectance from the iridophores was modeled using finite-difference time-domain (FDTD) methods. Using idealized spacings and orientations from SEM data from the lookdown skin, the spectra of this distribution was calculated and compared with the reflectance of lookdown skin. This resulted in a newly revealed method for fish to produce a broadband reflectance. (Cummings, Kattawar, Fig. 11; from Zhao et al. 2015)

7) We have developed two approaches for quantifying organismal pattern: A) We focus on three measures derived from the graylevel co-occurrence matrix, a type of luminance spatial covariance matrix for the image. These are (i) *contrast*, which measures the number of local grayscale transitions in the image; (ii) *energy*, which assesses object homogeneity, and (iii) *correlation*, which indicates the degree of gray level similarity in neighboring pixels. Fourth, we also consider object (iv) *entropy*, which quantifies the degree of disorder in the object. B) To compare object pixels to background, we employ an information theoretic approach. Our metric is based on the *mutual information* common in the neuroimaging field, which measures the reduction in uncertainty in one random variable when a second one is observed. We compute a mutual information image by using an object mask to select object pixels, and then compute for background pixels selected by translating the organismal mask to another part of the image. This is repeated by centering the background selection mask at every pixel in the image. These approaches have been worked into a matlab toolbox that is currently being applied to imagery collected during the field campaigns and will be freely available once published. (Dierssen)

8) Camouflage studies on *Sargassum* crabs were refined and (Fig. 12 A, B) were found to be extremely well matched to their background over most of the visible spectrum (Fig. 12 C, D). Crabs were indistinguishable from algae to a dichromatic fish predator model, while tetrachromat birds were able to discriminate between the color of crabs and algae due to far-red sensitivity. The ability to more closely match their algal background from visual detection by a fish compared to a bird potentially suggests that *Sargassum* crab camouflage may be driven more by predation by fish than birds. In *P. sayi*, the ability of an individual to match the color of its background is improved with size (Fig. 12E), while the opposite trend is observed in *P. minutus* (Fig 12F). The Sargassum crab *Portunus sayi* shows a diel cycle of coloration, being pale at night and darker during the day. Against monochromatic backgrounds, *P. sayi* displayed marked change in reflectance and contrast to predator visual systems with relatively short (12 hour) exposure. (Dierssen)

9) Results from the field trip (Curacao), additional lab experiments (Fig.13) and Monte Carlo simulations for elaboration of the beam spread function (BSF) for polarized light are combined to develop a simplified underwater polarimetric imaging model which is used for the analysis of the polarimetric images of a manmade underwater target with known polarization properties acquired by a full Stokes vector imaging camera in a field experiment. Significant differences between polarization characteristics of the target and its image were found even in clear waters

A method to retrieve both the inherent optical properties of the water (attenuation coefficient c) and the polarization characteristics of the target was explored and its efficacy is demonstrated for both laboratory and field experiments (Fig. 14). (Gilerson)

IMPACT/APPLICATIONS

New technology (in-situ holographic microscope) that was leveraged/developed to explore innovative methods to better understand the factors (i.e. particle dynamics) that control the spatial-temporal dynamics of the underwater polarized light field (MURI goal) has resulted in finding ubiquitous particle orientation in the coastal oceans and to new ONR funding (Sullivan, Twardowski, Kattawar).

The in-field polaro-crypsis measurements give material scientist a template from which to potentially create a new man-made material that would optimally camouflage under all viewing angles.

Peripheral vs. central control mechanisms for chromatophores remains an important open question. Central vs. peripheral (distributed) control is a basic property of most, if not all, complex systems and is thus of fundamental importance to many aspects of both the natural and man-made world.

RELATED PROJECTS

Sullivan, Twardowski and Kattawar have received funding from ONR for a project titled "Effects of natural, undisturbed particle fields on light transmission and dispersion in coastal waters." (ONR project N0001414C0267). The goal of this project is to better understand the links between particle dynamics and the spatial-temporal dynamics of the underwater polarized light field and is very synergistic with those of the MURI.

Cummings and Kattawar have been working on a related project developing a videopolarimetry mooring device enabling on-board (rather than diver-operated) ocean polarization measurements (Cummings, Kattwar, Gruev NSF OCE-1130793, 8/2011-8/2016

Synergistic 3-D spectral modeling in seagrass canopies has been undertaken as part of a follow-on research funded by NASA Ocean Biology and Biogeochemistry in collaboration with John Hedley (Environmental Computer Science, Ltd). Modeling to be presented at Ocean Optics XXII (Dierssen)

Hyperspectral airborne PRISM imagery has been obtained over the Florida Bay shallow water stations in collaboration with NASA Jet Propulsion Laboratory and Ocean Biology and Biogeochemistry. The benthic reflectance spectra obtained as part of the MURI are being incorporated into modeling algorithms for retrieving bottom depth and composition.

Supported projects to continue with squid chromatophore work:

"EAGER: Natural Chromogenic Behaviors of Squid in Oceanic Waters" – Proposal awarded by NSF ($250,000, 2 years, Gilly and Rosen)

"Natural behaviors of free-swimming Dosidicus gigas studied with an animal-born- video package and data loggers" – Proposal awarded by National Geographic CRE ($5,000,1year, Rosen and Gilly)

"Natural behaviors of Humboldt squid in relation to oxygen-limited habitats" – Proposal awarded by National Geographic CRE ($25,000, 1 year, Gilly and Rosen)

"Collaborative Research: Structural and functional connectivity of squid chromatophores" – Proposal submitted to NSF ($682,916, 3 years, Gilly & Rosen; $386,761, 3 years, J. Rosenthal, Univ. Puerto Rico).

REFERENCES

Aas E. The refractive index of phytoplankton, Rep. 46, 61 pp. Inst Geophys, Univ of Oslo, Oslo, Norway. 1981.

Aas E. Refractive index of phytoplankton derived from its metabolite composition. J Plankton Res 1996;18:2223-49.

Sun B, Yang P, Kattawar GW. Many-Body Iterative T-matrix Method for Large Aspect Ratio Particles. J Quant Spectrosc Radiat Transfer. 2013;127:165-75.

Yan W-Z, Du Y, Wu H, Liu D, Wu B-I. EM scattering from a long dielectric circular cylinder. Prog Electromagn Res 2008;85:39-67.

Yang P, Liou K. Light scattering by hexagonal ice crystals: solutions by a ray-by-ray integration algorithm. J Opt Soc Am A 1997;14:2278-89.

PUBLICATIONS

Brady P, Gilerson A, Kattawar G, Sullivan J, Twardowski M, Dierssen H, Gao M, Travis K, Etheredge RI, Tonizzo A, Ibrahim A, Carrizo C, Gu Y, Russel B, Mislinski K, Zhao S, Cummings ME. (*in press*) Open ocean fish reveal an omnidirectional solution to camouflage in polarized environments. *Science* [published; refereed]

Bell, George RR, Lydia M. Mäthger, Meng Gao, Stephen L. Senft, Alan M. Kuzirian, George W. Kattawar, and Roger T. Hanlon. "Diffuse white structural coloration from multilayer reflectors in a squid." *Advanced Materials* 26, no. 25 (2014): 4352-4356. [published, refereed]

Churnside, J. H., J. M. Sullivan & M. S. Twardowski (2014) - Lidar extinction-to-backscatter ratio of the ocean. Optics Express, 22(15): 18698-18706. [published, refereed]

Dierssen, H.M., A. Chlus, B. Russell. 2015. Hyperspectral discrimination of floating mats of seagrass wrack and the macroalgae Sargassum in coastal waters of Greater Florida Bay using airborne remote sensing. Remote Sens. Environ. 10.1016/j.rse.2015.01.027 [published, refereed]

Dierssen, H.M. and A.E. Theberge. 2014. Bathymetry: History of Seafloor Mapping. Encyclopedia of Natural Resources. Volume II: Water and Air. Taylor & Francis Group. New York. ISBN 9781439852583 [published, refereed]

Dierssen, H.M. and A.E. Theberge. 2014. Bathymetry: Assessing Methods. Encyclopedia of Natural Resources. Volume II: Water and Air. Taylor & Francis Group. New York. ISBN 9781439852583 [published, refereed]

Dierssen, H.M. and A.E. Theberge. 2014. Bathymetry: Features and Hypsography. Encyclopedia of Natural Resources. Volume II: Water and Air. Taylor & Francis Group. New York. ISBN 9781439852583 [published, refereed]

Y. Gu, C. Carrizo, A. A. Gilerson, P. Brady, M. E. Cummings, M. S. Twardowski, J. M. Sullivan, A. Ibrahim, and G. W. Kattawar, "Polarimetric imaging and retrieval of target polarization

characteristics in underwater environment,“ Applied Optics, 2015, submitted.[submitted, refereed]

Y. Gu, C. Carrizo, A. El-Habashi, and A. Gilerson, “Analysis of Polarimetric Image by Full Stokes Vector Imaging Camera for Retrieval of Target Polarization in Underwater Environment,” Proc. of SPIE, 9459, 2015. [published, refereed]

A. Gilerson, A. Ibrahim, R. Foster, C. Carrizo, A. El-Habashi and S. Ahmed, “Retrieval of water optical properties using polarization of light underwater: Case I and II waters, “ Proc. of SPIE, 9240, 2014. [published, refereed]

Huang, Xin, Ping Yang, George Kattawar, and Kuo-Nan Liou. "Effect of mineral dust aerosol aspect ratio on polarized reflectance." *Journal of Quantitative Spectroscopy and Radiative Transfer* 151 (2015): 97-109. [published, refereed]

A. Ibrahim, A. Gilerson, J. Chowdhary, and S. Ahmed, “Retrieval of macro- and micro-physical properties of oceanic hydrosols from polarimetric observations,” Remote Sensing of Environment, 2015, submitted. [submitted, refereed]

Rosen H, Gilly W, Bell L, Abernathy K, Marshall G. 2015. Chromogenic behaviors of Humboldt Squid, *Dosidicus gigas* (d’Orbigny, 1835), studied *in situ* with an animal-borne video package. J. Exp. Biol. 218: 265-275 [published, refereed]

Mislinski KR, Brady P, Etheredge RI, Gruev V, Cummings ME. Polarized reflectance of marine fish from different habitats—and examination of habitat-dependent polaro-crypsis. PLoS ONE [submitted; refereed]

Russell, B. and H. M. Dierssen. 2015, Use of Hyperspectral Imagery to Assess Cryptic Color Matching in Sargassum Associated Crabs. Plos One. [Published, refereed]

Sun, Bingqiang, Ping Yang, George W. Kattawar, and Lei Bi. "Scattering of 1-D periodic scatterer and asymptotic comparison using the many-body iterative T-matrix method." *Journal of Quantitative Spectroscopy and Radiative Transfer* 146 (2014): 459-467. [published, refereed]

Yi, Bingqi, Xin Huang, Ping Yang, Bryan A. Baum, and George W. Kattawar. "Considering polarization in MODIS-based cloud property retrievals by using a vector radiative transfer code." *Journal of Quantitative Spectroscopy and Radiative Transfer* 146 (2014): 540-548. [published, refereed]

Zhao, S., Brady, P. C., Gao, M., Etheredge, R. I., Kattawar, G. W., & Cummings, M. E. (2015). Broadband and polarization reflectors in the lookdown, Selene vomer. *Journal of the Royal Society Interface*, *12*(104), 20141390. [published, refereed]

HONORS/AWARDS/PRIZES

George W. Kattawar of TAMU won the Jerlov Award of The Oceanography Society for 2014

George W. Kattawar of TAMU won the van de Hulst Light Scattering Award 2015 presented by Elsevier.

FIGURES

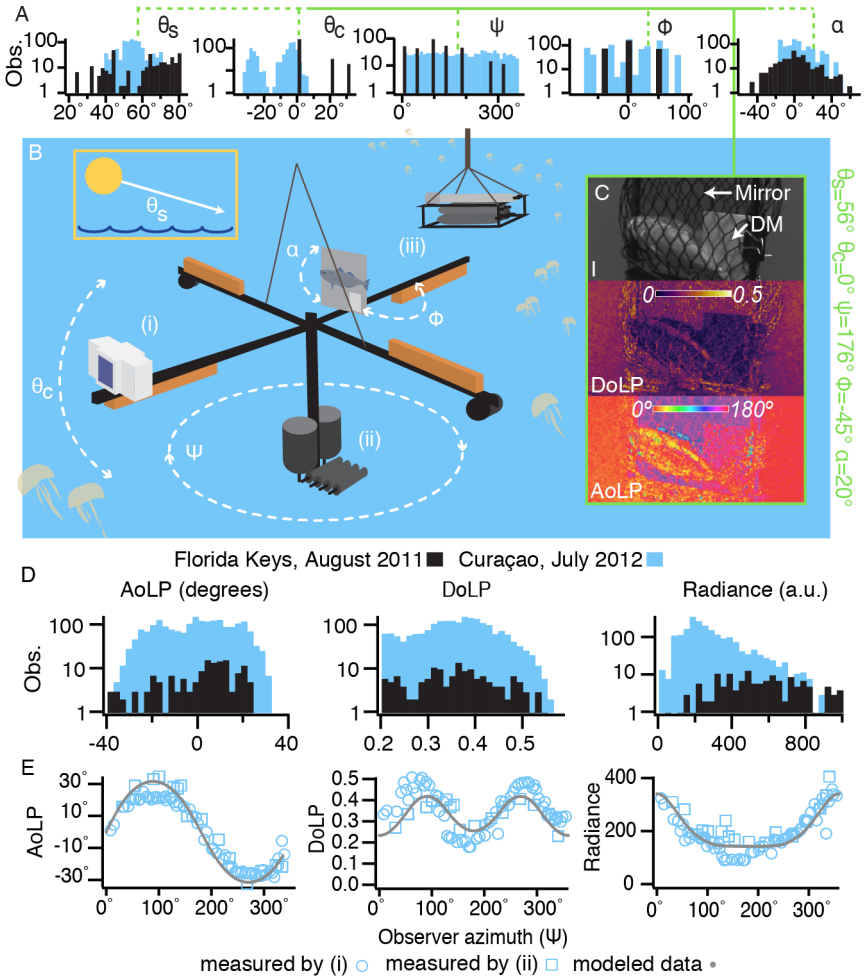

Figure 1. Angular configuration of >1500 in field measurements of live fish in open ocean water conditions (A) collected at different angular configurations of solar angle (θ_s), camera inclination angle (θ_c), camera azimuth angle (ψ), relative yaw angle (φ), and fish pitch angle (α) from Florida Keys (black) and Curaçao (blue). (B) Measurements were obtained with a (i) videopolarimeter (Cummings) utilizing a remotely operated underwater rotating platform (Gilerson) and validated by measurements with (ii) a hyperspectral radiometric polarimeter (Gilerson)and (iii) inherent optical properties simultaneously recorded (Sullivan, Dierssen). In Curaçao, integrated digital compass and inertial sensors (Cummings) with the videopolarimeter provided nearly continuous azimuth (ψ) and pitch (θ_c) angle measurements. (C) Polarimetric image of a bigeye scad restrained against Mirror and Diffuse Mirror (DM) shown in radiance (I), Degree of linear polarization (DoLP), and Angle of Linear Polarization (AoLP). (D) Azimuthal (ψ) background measurements of the water column AoLP, DoLP and radiance in Curaçao (blue) and Florida (black). (E) Measurements and simulations of the background light field for a single azimuthal rotation (3 minutes)

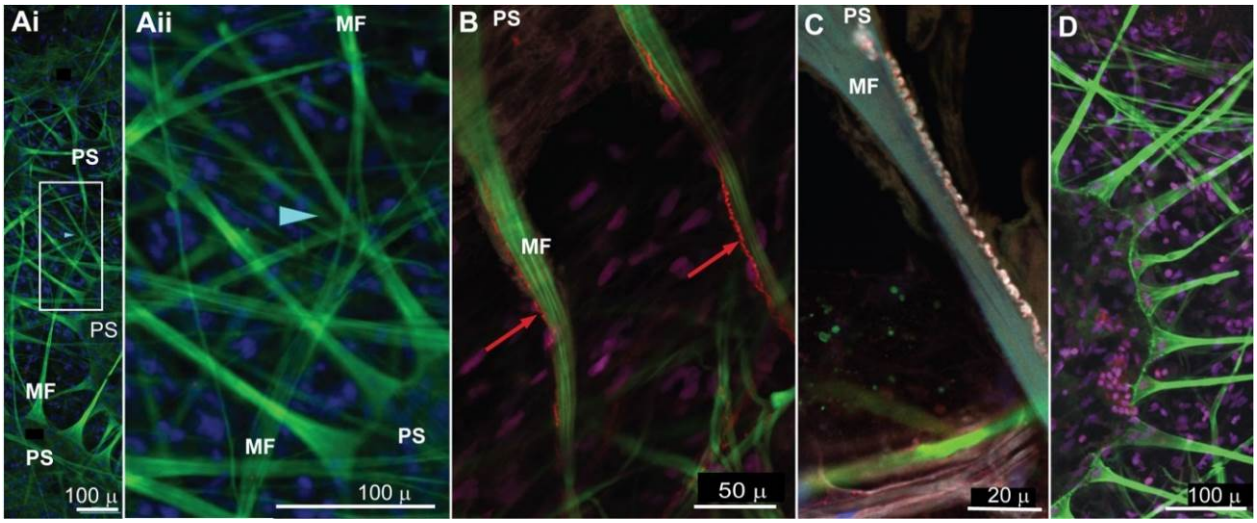

Figure 2. Chromatophore structure in Doryteuthis opalescens. A. Labelling of F-actin (green) in muscle fibers (MF) with Alexa Fluor 488 (Life Sci. Tech. A12379;1:250 dilution; 3 hr incubation) and nuclear DNA with1:50 DAPI (blue). Pigment sacs (PS) are indicated. 2 hr fixation. Boxed region in panel Ai is expanded in Aii. B. Labeling as in A) plus labeling of 5HT (red) with polyclonal anti-5HT (Sigma S5545; 1:200, 3hr) and anti-rabbit secondary (Alexa Fluor 546; 1:250, 2 hr). Serotonergic axons run along radial muscle fibers (arrows). PS lies at top. 4 hrs fix. C. Labelling as in B) plus labeling of L-Glu with monoclonal anti-glutamate (Sigma G9282; 1:20,000, 3 hr) and anti-mouse secondary (Alexa Fluor 647; 1:250, 2 hr). 5HT antiserum was used at 1:500. 4 hrs fix with additional 0.1% glutaraldehyde. D. Unilateral denervation 7 days prior to fixation. Labeling as in C). Serotonergic axons associated with muscle fibers have degenerated. 2 hrs fix. Methods: Skin from the dorsal mantle (1-2 cm2) was pinned out, and the epidermis and irridophore layer were removed by dissection. The chromatophore layer was fixed in 4% paraformaldehyde in seawater for 2-4 hours at 20°C, washed with PBS + 0.01% Na azide and stored at 4°C for up to 7 days. Samples were treated with 5mg/ml collagenase (Gibco Type 1) for 30 min. at 37°C before labeling procedures. Whole-mounts were examined with a Zeiss 700 confocal microscope.

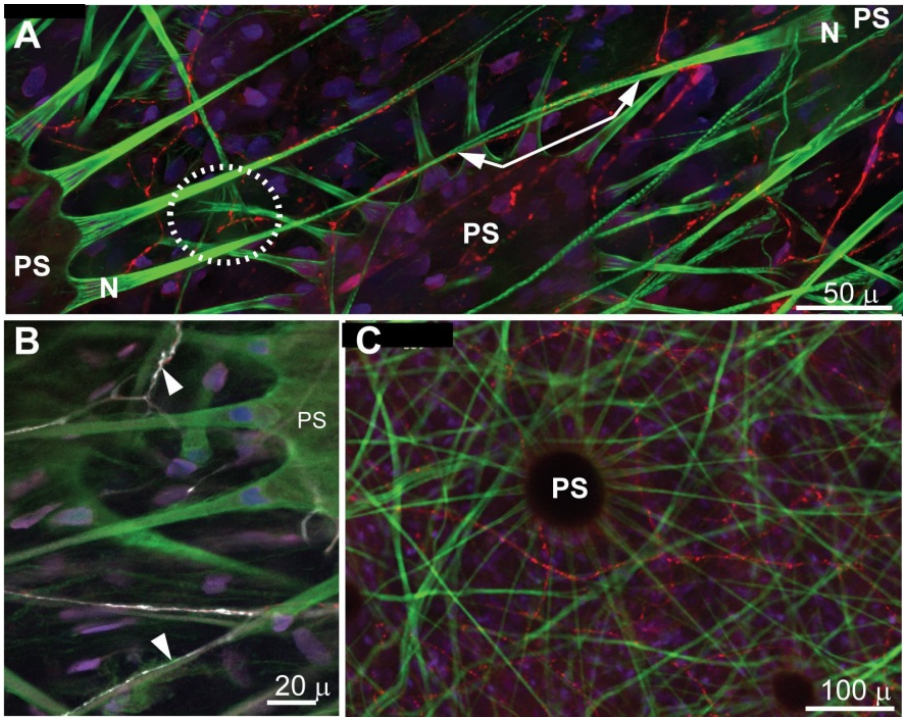

Figure 3. Chromatophore structure in Dosidicus. A. Labeling of F-actin, nuclear DNA and 5HT were carried out as described in conjunction with Fig. 1. Serotonergic axons are red. Distal branching of two muscle fibers is circled. Arrows joined by the line indicate a potential connection between muscle fibers from neighboring chromatophores. B. Labeling as in panel A plus anti-glutamate (white). Glutamatergic axons running along muscle fibers are indicated by arrowheads. Serotonergic processes are not visible in this image. C. Labeling as in panel A. Low-power view showing the general, diffuse pattern of the serotonergic innervation.

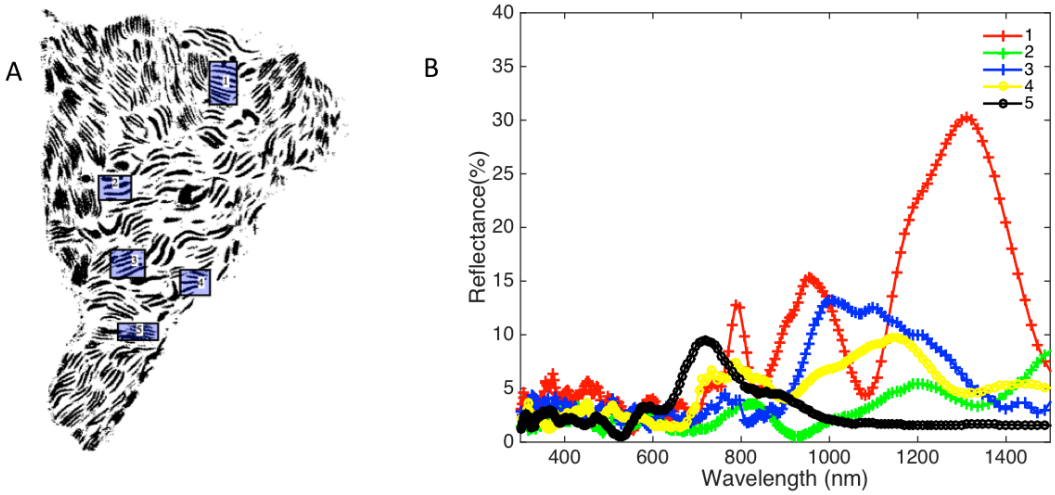

Figure 4. Spectral reflectance of sub-regions in an iridophore cell

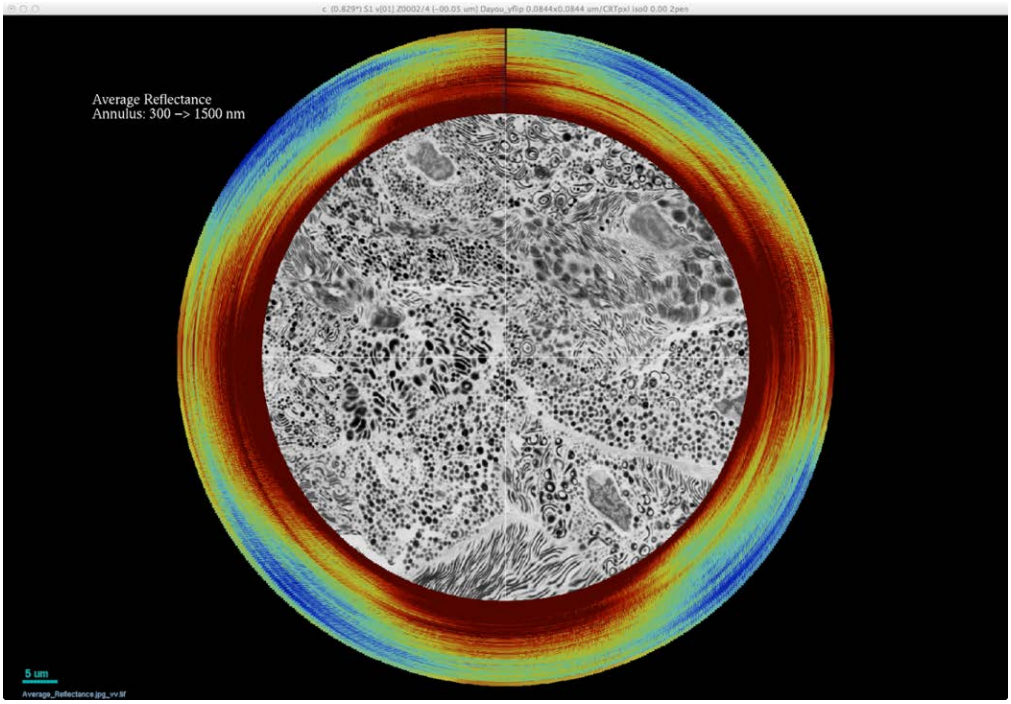

Figure 5. Spectral reflectance of a circular region from cuttlefish fin spot at different incident directions

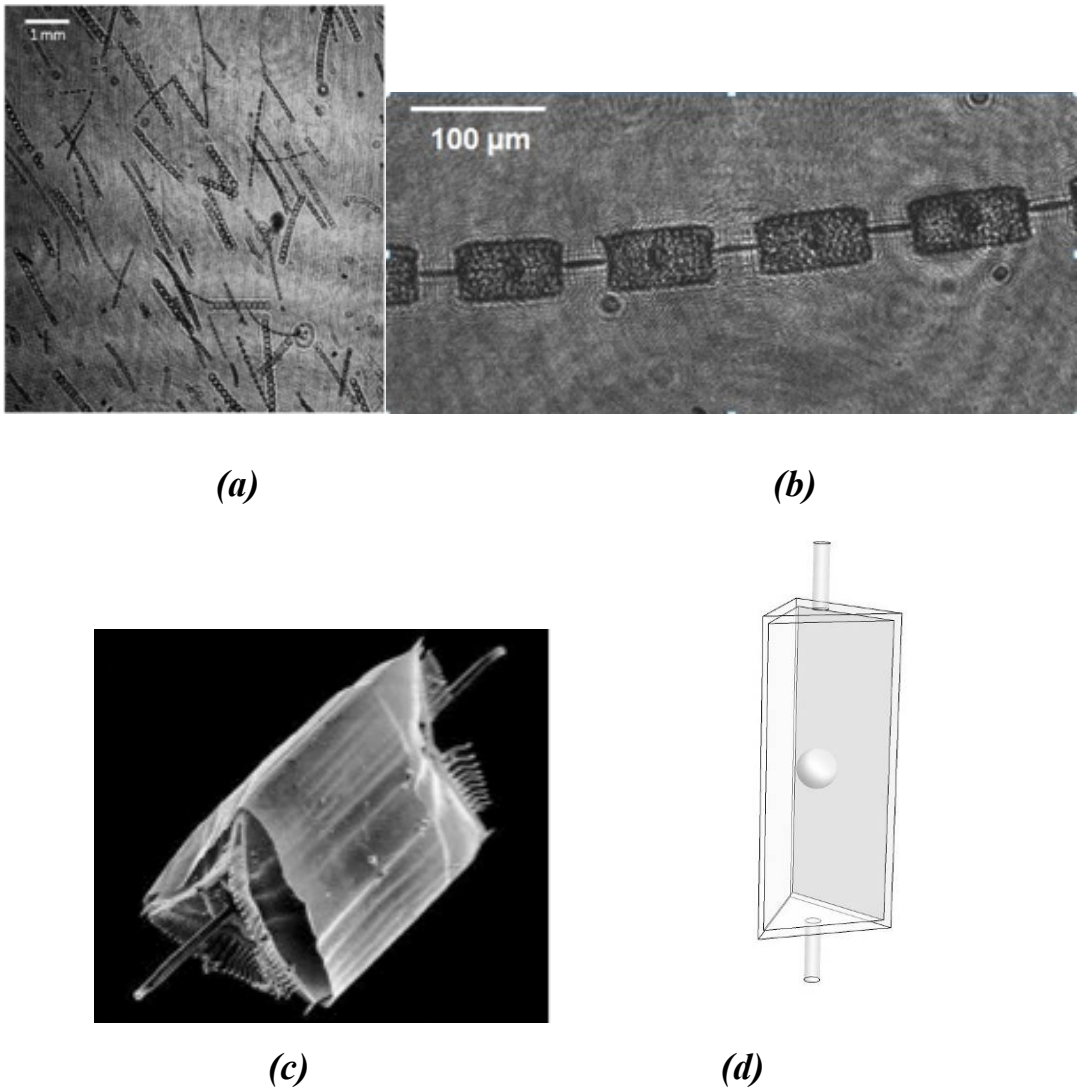

Figure 6. Different scale views of the diatom Ditylum sp: (a) linear chains of diatoms in the ocean; (b) a single diatom chain; (c) the SEM image of a single diatom cell [6]; and, (d) the simulation model.

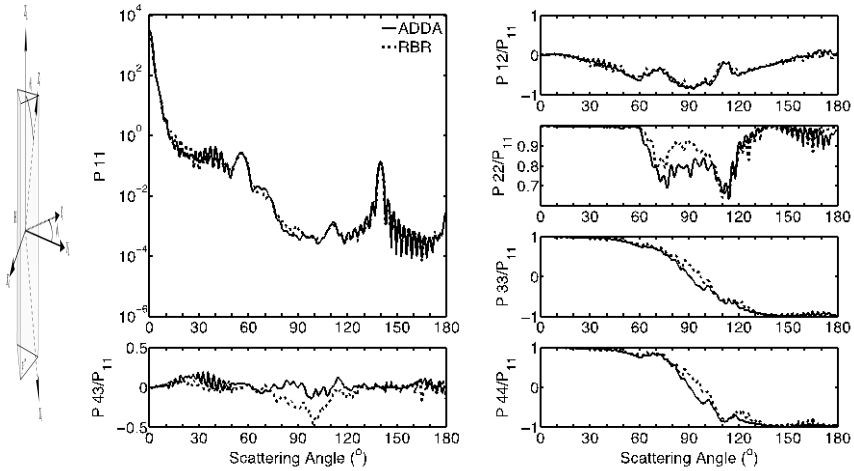

Figure 7. (left) The laboratory frame of reference with the z-axis along the prism's main axis and the x-axis perpendicular to one of the prism side surfaces and pointing inside to the corresponding prism edge, and an interpretation of the relative incident angles. H indicates the prism height and r is the distance from the prism lower center to the vertex. (right) Comparison between the Mueller Matrix elements of one cell calculated by the ADDA and the RBR. The outer prism height H and radius r are 9µm and 4.5µm, the inner prism height H and radius r are 8.58 µm and 4.29µm, the core radius is 0.57µm, the spine length and diameter are 1.8µm and 0.45µm, the incident wavelength is 0.475µm, and the incident angles are $\theta_i = 70^0, \varphi_i = 0^0$.

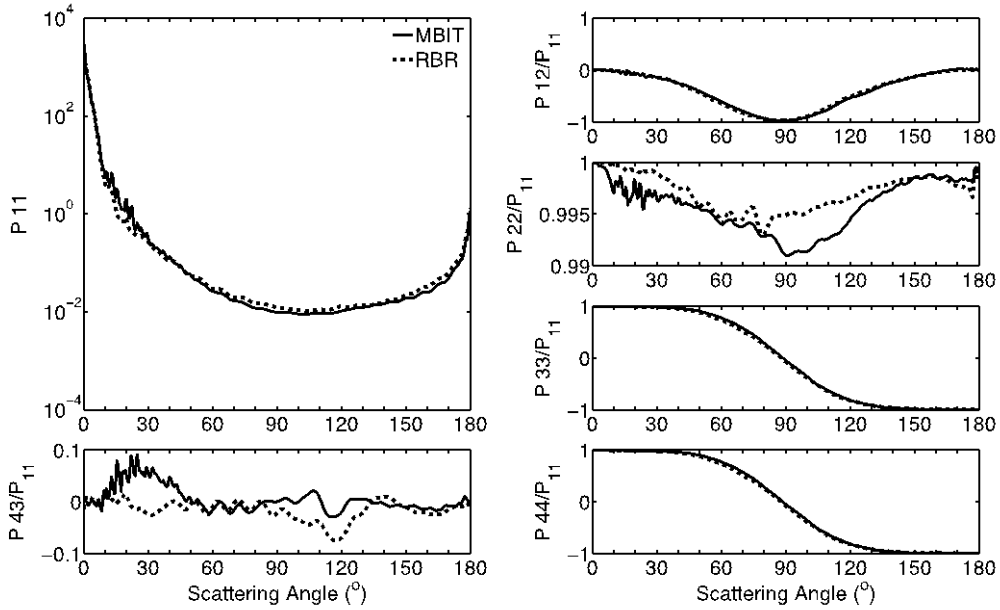

Figure 8. Comparison between the Mueller Matrix elements of two diatom cells calculated by the MBIT and the RBR. The outer prism height H and radius r are 9µm and 2.25µm, the inner prism height H and radius r are 8.58µm and 2.04µm, the core radius is 0.57µm, and the spine length and diameter are 1.8µm and 0.45µm, the incident wavelength is 0.475µm, and the incident zenith angle θ_i ***is*** 90^0 ***with the result averaged by the incident azimuthal angles*** φ_i ***from*** 0^0 ***to*** 60^0.

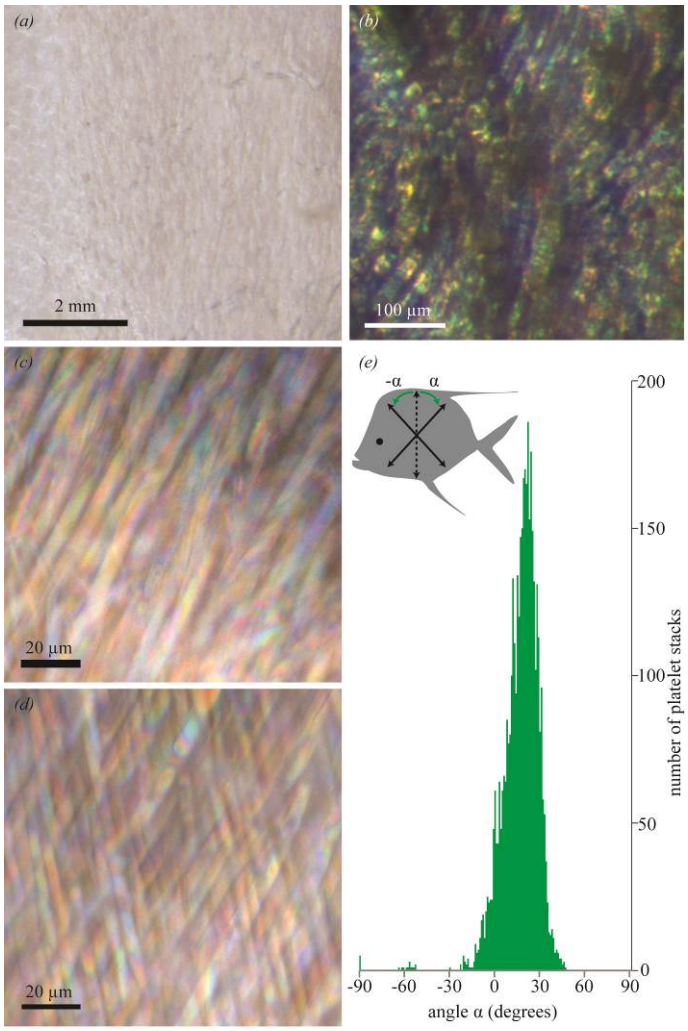

Figure 9. Skin preparations and pitch angles of guanine platelets' (a) A low-magnification image shows the silvery skin from the ventrolateral flank. (b) A higher-magnification image of the same region as in (a) shows multiple color patches and the effect of rings of the scales. (c) Removal of the scales and the collagen layer revealed stacks of multi-colored Type 3 guanine platelets in the mid-lateral flank with epi-illumination. The guanine platelets were oriented predominantly in one direction. (d) In some areas of the mid-lateral skin, two distinct orientations of Type 3 platelets were observed. (e) With the fish head on the left and the tail on the right, the pitch angle of a platelet (alpha) is defined as positive or negative if it is tilted away from the vertical line clockwise or counter-clockwise, respectively. Pitch angles of the guanine platelets in the mid-lateral flank show an average of 17.3^o ± 11.0^o (mean ± SD) and the peak between 22° and 23°. (Zhao 2015)

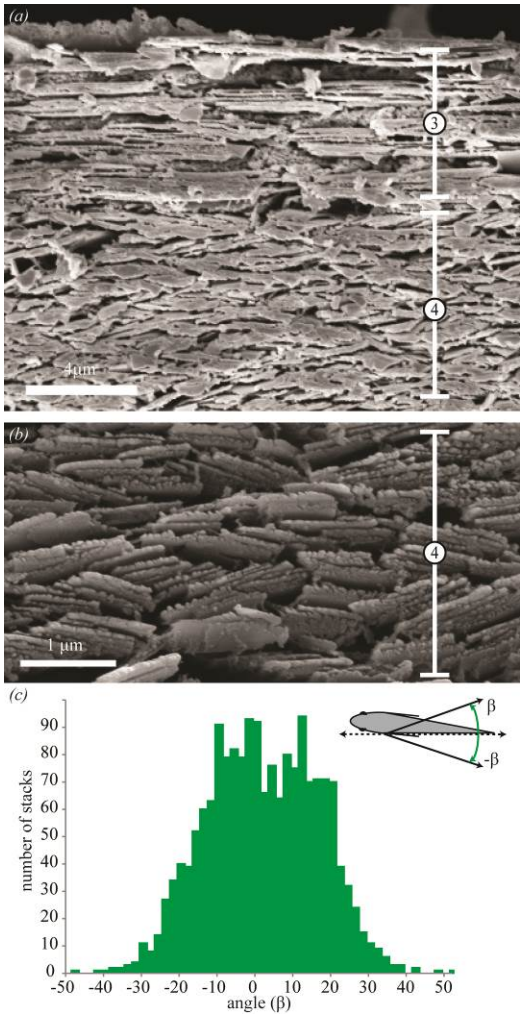

Figure 10. Yaw angles of the guanine platelets. (a) SEM image of a horizontal section from the mid-lateral flank shows that the short axes of the Type 3 platelets are paralleled to the skin surface (horizontal) while those of Type 4 platelets exhibit various orientations. (b) A higher-magnification image of Type 4 platelets shows random orientations of their short axes. (c) Definition of positive (beta) and negative (-beta) yaw angles between the fish surface and the short axes of the platelets and the histogram of the yaw angles. The solid line is fitting of the data to normal distribution. The average angle was $0.59^o \pm 14.59^o$ (mean ± SD, n = 1761). (Zhao 2015)

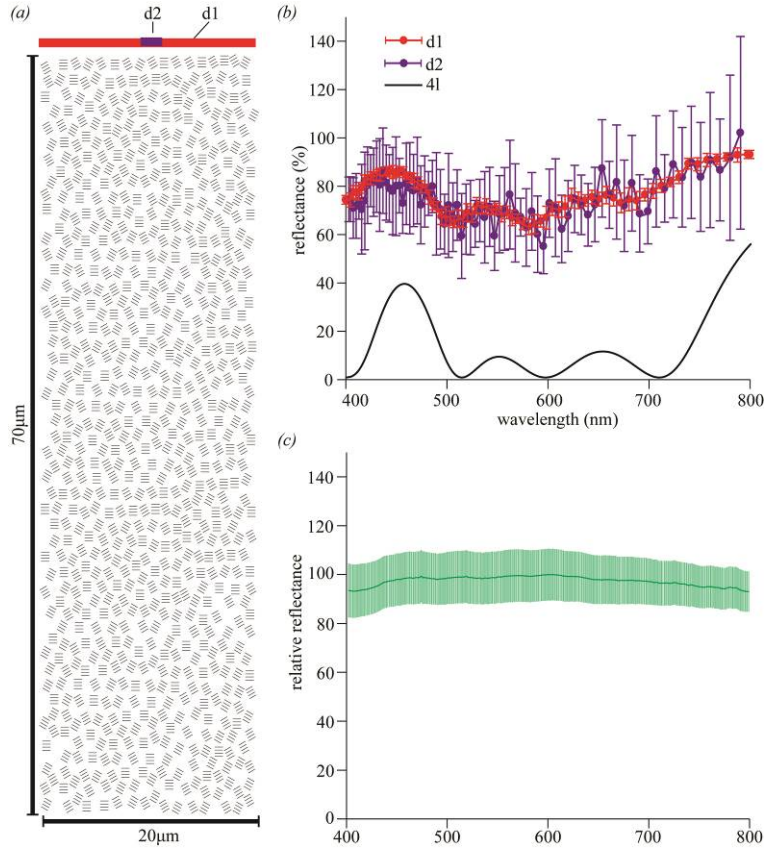

Figure 11. Reflectance from simulation and measurement. (a) The configuration of guanine platelet stacks for simulation. Each stack consists of four individual platelets. The orientation of the stacks follows the Gaussian distribution. The widths for detectors d1 and d2 are 20 μm and 2 μm, respectively. (b) Average reflectance from simulations of 10 randomly generated configurations. Error bars represent standard deviations. Reflectance detected by d1 is a relatively flat spectrum with small variations. Average reflectance detected by d2 is similar to that by d1, but with much greater variations. This suggests that color variation between small areas is very likely. The black solid line shows the reflectance spectrum (by d1) of 4 layer platelets (4l) with the same dimension as the platelet stack in (a) but all parallel with the surface and with an infinite radius. (C) Relative reflectance measured from the ventral flank of the lookdown. The dark green line is the average spectrum of nine measurements. The light green shade marks the standard deviations of the measurements. (Zhao 2015)

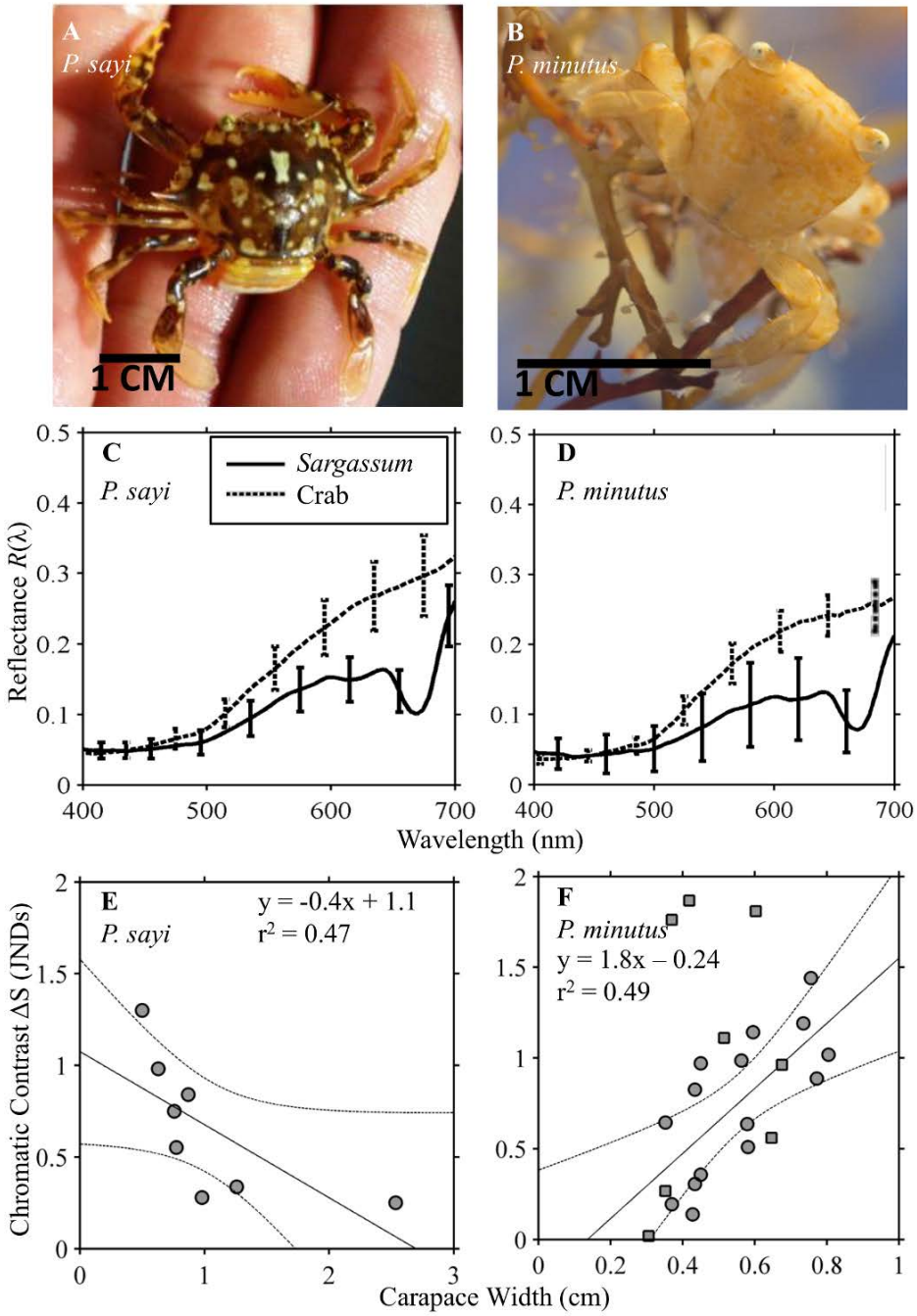

Figure 12. The Sargassum crabs P. sayi (A) and P. minutus (B). Both species closely match the reflectance of the Sargassum algae (C, D) in blue/green wavelengths, but diverge in the red, with the greatest difference in the secondary chlorophyll absorbance band (~675 nm). A chromatic model shows that for fish predators, P. sayi (E) show improved color matching (decreasing chromatic contrast) with size, while the opposite trend was present in P. minutus (F).

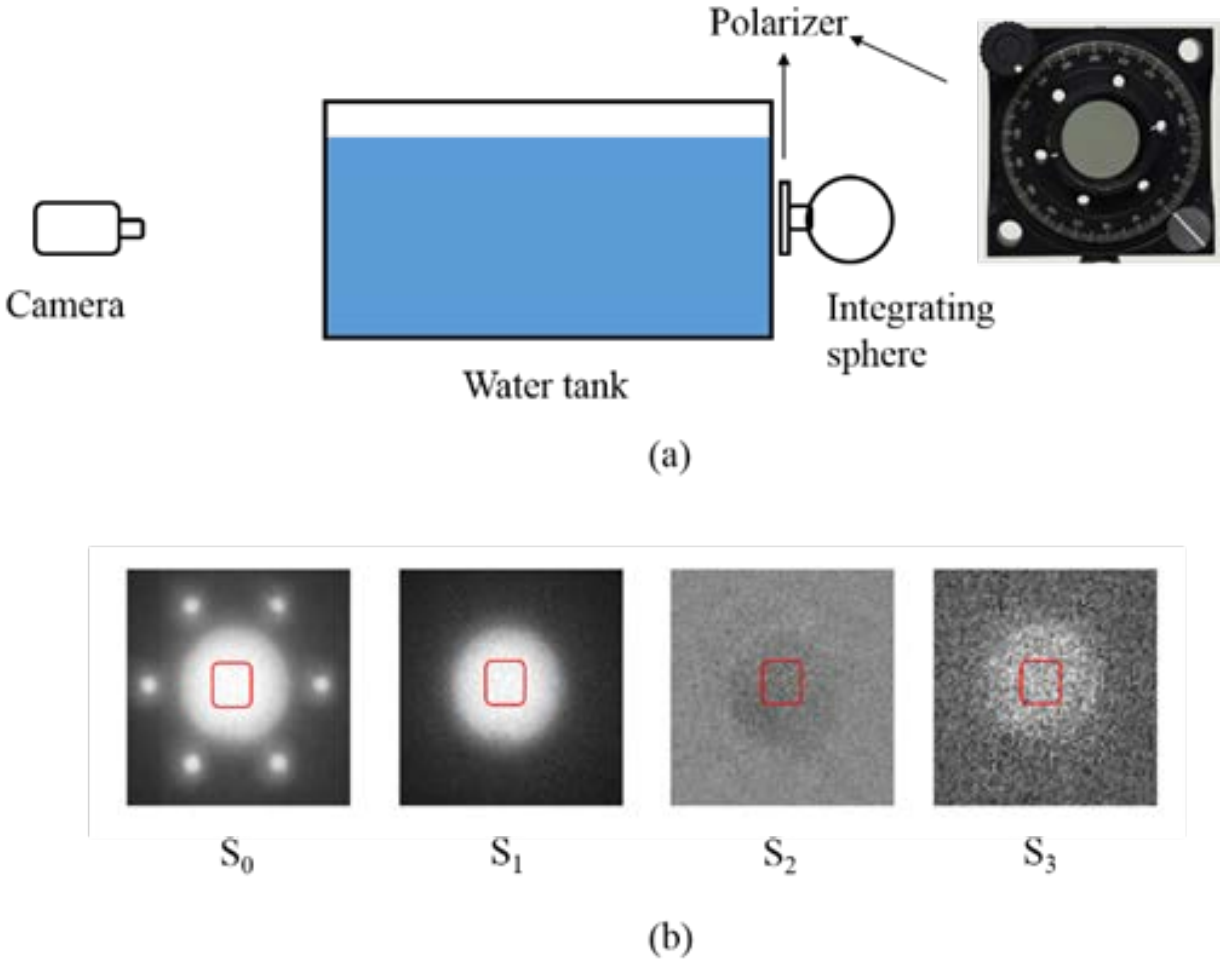

Figure 13. (a) Experiment setup for polarization measurement of the light after passing through a 0° linear polarizer and the water tank. (b) The full Stokes vector image of a measurement demonstrating that the magnitude of S2 and S3 Stokes components is much smaller than of S0 and S1.

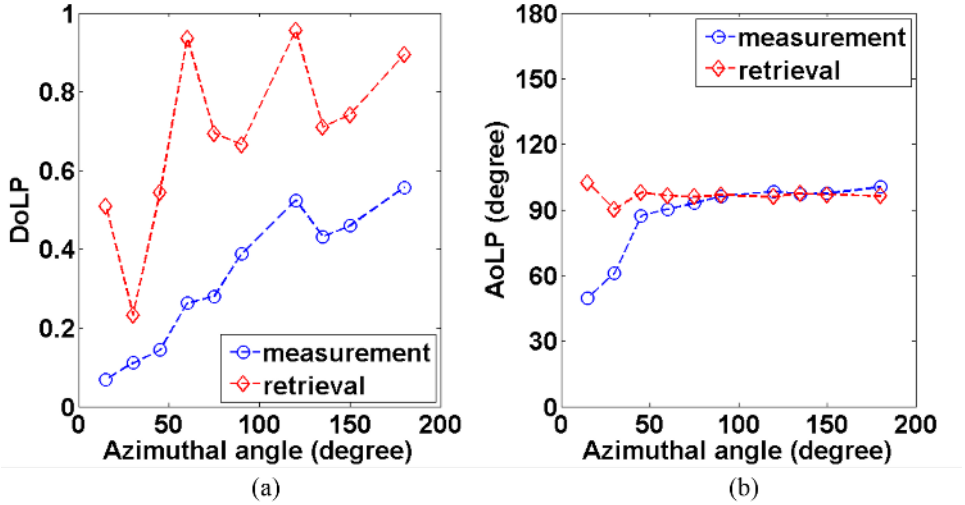

Figure 14. Measured and retrieved DoLP (a) and AoLP (b) of the 90° polarizer. The data for the measured plots are from the pixels of the Stokes vector image corresponding to the 90° polarizer. The data were acquired at one of the stations during Curacao field trip.